2016 IEEE International Conference on Robotics and Automation (ICRA)
Stockholm, Sweden, May 16-21, 2016

Experimental Implementation of Underactuated Potential Energy Shaping on a Powered Ankle-Foot Orthosis

Ge Lv*, Hanqi Zhu*, Toby Elery, Luwei Li, and Robert D. Gregg

Abstract— **Traditional control methodologies of rehabilitation orthoses/exoskeletons aim at replicating normal kinematics and thus fall into the category of *kinematic control*. This control paradigm depends on pre-defined reference trajectories, which can be difficult to adjust between different locomotor tasks and human subjects. An alternative control category, *kinetic control*, enforces kinetic goals (e.g., torques or energy) instead of kinematic trajectories, which could provide a flexible learning environment for the user while freeing up therapists to make corrections. We propose that the theory of underactuated potential energy shaping, which falls into the category of kinetic control, could be used to generate virtual body-weight support for stroke gait rehabilitation. After deriving the nonlinear control law and simulating it on a human-like biped model, we implemented this controller on a powered ankle-foot orthosis that was designed specifically for testing torque control strategies. Experimental results with an able-bodied human subject demonstrate the feasibility of the control approach for both positive and negative virtual body-weight augmentation.**

I. INTRODUCTION

Lower-limb orthoses and exoskeletons have been developed with different structures and control strategies to assist users during their locomotion. Rehabilitation orthoses and exoskeletons are tools that aim to relieve the repetitive and physically tasking duties of the clinicians and therapists as well as improving the patient's recovery efficacy [1]. Traditional control methodologies for rehabilitation exoskeletons are designed to replicate normal kinematics (joint angles/velocities) and thus fall into the category of *kinematic control*. This approach is especially useful for providing assistance to individuals with spinal cord injury, who cannot contribute to the kinematic patterns of their own legs. Many exoskeletons have adopted this control paradigm to generate missing function for the user's lower limbs, e.g., [2]–[7]. Even though these devices have shown promising results, their controllers force patients to follow pre-defined walking patterns, which may not be desirable for patients with some control of their lower limbs, such as stroke patients [8].

An alternative control category, *kinetic control*, enforces kinetic goals (e.g., torques or energy) instead of kinematic trajectories, which might provide more flexible gait training paradigms. Instead of constraining a patient's motion in a pre-defined manner, kinetic control could provide a supportive environment to allow the patient to relearn their own personal, preferred gait. However, very few methods exist for kinetic control of exoskeletons, which almost exclusively utilize kinematic strategies that compensate for chronic deficits instead of enabling recovery of patient's normative gait [9]. Related to kinetic control, although not designed for physical rehabilitation, the BLEEX enhances the ability of an able-bodied user to carry extra heavy loads, using force control to minimize the user's interaction forces with the exoskeleton so the user does not feel the weight of the backpack [10]. However, minimizing interaction forces with the exoskeleton does not offload the body weight of the human user as needed in rehabilitation. Kinetic control methods that could enable greater flexibility for powered exoskeletons need to be developed for gait rehabilitation systems.

To address this issue, we propose that the nonlinear control method of *potential energy shaping* [11] is ideally suited for kinetic control of exoskeletons. By altering the potential energy of the human dynamics in closed loop, body-weight support (BWS) can be provided virtually through the actuators of powered lower-limb exoskeletons, allowing patients to train their walking motions naturally with less perceived gravity as well as freeing up therapists to make corrections. However, the changing contact conditions and degrees of underactuation encountered during human walking present significant challenges to consistently matching a desired potential energy for the human in closed loop. Therefore, we are investigating contact-invariant ways of matching desired dynamics to enable exoskeletal BWS, and we have demonstrated beneficial effects of this control methodology in simulations of a powered knee-ankle orthosis on a human-like biped model [12], [13]. This feedback control strategy is fundamentally task-invariant, and its parameterization allows systematic adjustments for patient-specific therapy.

This paper presents the first experimental validation of the potential energy shaping approach, which is implemented in a highly backdrivable, torque-controlled powered ankle-foot orthosis (PAFO). We begin in Section II by modeling the orthosis dynamics with contact constraints corresponding to heel contact, flat foot, toe contact, and no contact (i.e., swing). In Section III, energy shaping control laws are derived for the ankle actuator to provide virtual BWS to a human subject. Torque profiles from simulations provide a reference for the PAFO hardware design. Then, Section IV presents the mechanical and electronic design of the PAFO and validates its closed-loop torque control capabilities for

Asterisks indicate both authors contributed equally.

G. Lv, H. Zhu, and L. Li are with the Department of Electrical Engineering, T. Elery is with the Department of Mechanical Engineering, and R. D. Gregg is with the Departments of Bioengineering and Mechanical Engineering, University of Texas at Dallas, 800 W. Campbell Road, Richardson, TX 75080, USA. {Ge.Lv, Hanqi.Zhu, rgregg}@utdallas.edu

This work was supported by the National Institute of Child Health & Human Development of the NIH under Award Number DP2HD080349. The content is solely the responsibility of the authors and does not necessarily represent the official views of the NIH. R. D. Gregg holds a Career Award at the Scientific Interface from the Burroughs Welcome Fund.

implementing the potential energy shaping controller. An able-bodied human subject experiment with this PAFO is presented in Section V, demonstrating the feasibility of the potential energy shaping approach for both positive and negative virtual body-weight augmentation.

II. Modeling the Leg Dynamics

We are interested in controlling a powered ankle-foot orthosis using only feedback local to its leg. We will find it convenient to separately model the dynamics of the stance and swing legs, which are coupled through interaction forces (Fig. 1). For simplicity we assume that 1) upper body masses are lumped together in the hip mass of the stance leg model, and 2) the masses m_i, $i \in \{\mathrm{f}, \mathrm{s}\}$, are the combined masses of the human limb and its orthosis.

A. Stance Leg Dynamics

The stance leg is modeled as a 5 degree-of-freedom (DOF) kinematic chain with respect to an inertial reference frame (IRF) defined at either the heel or toe, depending on the phase of the stance period (to be discussed later). The configuration of this leg is given by $q_{\mathrm{st}} = (p_{\mathrm{x}}, p_{\mathrm{y}}, \phi, \theta_{\mathrm{a}}, \theta_{\mathrm{k}})^T$, where p_{x} and p_{y} are the Cartesian coordinates of the heel, ϕ is the angle of the heel defined with respect to the vertical axis, and θ_{a} and θ_{k} are the angles of the ankle and knee, respectively. The Lagrangian dynamics can be derived in the form

$$M_{\mathrm{st}}(q_{\mathrm{st}})\ddot{q}_{\mathrm{st}} + C_{\mathrm{st}}(q_{\mathrm{st}}, \dot{q}_{\mathrm{st}})\dot{q}_{\mathrm{st}} + N_{\mathrm{st}}(q_{\mathrm{st}}) + A_{\ell}(q_{\mathrm{st}})^T\lambda = B_{\mathrm{st}}u_{\mathrm{st}} + B_{\mathrm{h}}v_{\mathrm{st}} + J_{\mathrm{st}}(q_{\mathrm{st}})^T F, \quad (1)$$

where M_{st} is the inertia/mass matrix, C_{st} is the Coriolis/centrifugal matrix, N_{st} is the gravitational forces vector. $A_\ell \in \mathbb{R}^{c\times 5}$ is the constraint matrix defined as the gradient of the constraint functions, c is the number of contact constraints that may change during different contact conditions, and $\ell \in \{\mathrm{heel}, \mathrm{flat}, \mathrm{toe}\}$ indicates the contact configuration. The Lagrange multiplier λ is calculated using the method in [14]. Assuming the orthosis has actuation at the ankle joint, i.e., u_{st}, the matrix $B_{\mathrm{st}} = (0_{1\times 3}, 1, 0)^T$ maps orthosis torque into the coordinate system. The interaction forces $F = (F_{\mathrm{x}}, F_{\mathrm{y}}, M_{\mathrm{z}})^T \in \mathbb{R}^{3\times 1}$ between the hip of stance model and the swing thigh are composed of 3 parts: two linear forces and a moment in the sagittal plane [14]. Force vector F is mapped into the system's dynamics by the *body Jacobian* matrix $J_{\mathrm{st}}(q_{\mathrm{st}}) \in \mathbb{R}^{3\times 5}$. The human input term $v_{\mathrm{st}} = [v_{\mathrm{a}}, v_{\mathrm{k}}]^T \in \mathbb{R}^{2\times 1}$ provides torques at the ankle and knee joints, i.e., v_{a} and v_{k}, which are mapped into the dynamical system through $B_{\mathrm{h}} = (0_{2\times 3}, I_{2\times 2})^T \in \mathbb{R}^{5\times 2}$. While designing the energy shaping controller, we make no assumptions about the human inputs or interaction forces.

During stance phase, the locomotion of the stance leg can be separated into three sub-phases: heel contact, flat foot, and toe contact, as depicted in Fig. 2, for which holonomic contact constraints can be appropriately defined.

1) Heel Contact: The heel is fixed to the ground as the only contact point, about which the stance leg rotates. The IRF is defined at the heel, yielding the constraint $a_{\mathrm{heel}}(q) = 0$ and the constraint matrix $A_{\mathrm{heel}} = \nabla_{q_{\mathrm{st}}} a_{\mathrm{heel}}$, where

$$a_{\mathrm{heel}} := (p_{\mathrm{x}}, p_{\mathrm{y}})^T \implies A_{\mathrm{heel}} = \left(I_{2\times 2}, 0_{2\times 3}\right). \quad (2)$$

2) Flat Foot: At this configuration the foot is flat on the ground, where ϕ is equal to the slope angle. The IRF is still defined at the heel, which yields the constraint $a_{\mathrm{flat}}(q) = 0$ and the constraint matrix $A_{\mathrm{flat}} = \nabla_{q_{\mathrm{st}}} a_{\mathrm{flat}}$, where

$$a_{\mathrm{flat}} := (p_{\mathrm{x}}, p_{\mathrm{y}}, \phi - \gamma)^T \implies A_{\mathrm{flat}} = \left(I_{3\times 3}, 0_{3\times 2}\right). \quad (3)$$

3) Toe Contact: The toe contact condition begins when the Center of Pressure (COP), the point along the foot where the ground reaction force is imparted, reaches the toe. During this phase the toe is the only contact point, about which the stance leg rotates. The IRF is defined at this contact point to simplify the contact constraints. The heel coordinates are then defined with respect to the toe, yielding the constraint $a_{\mathrm{toe}}(q) = 0$ and constraint matrix $A_{\mathrm{toe}} = \nabla_{q_{\mathrm{st}}} a_{\mathrm{toe}}$:

$$a_{\mathrm{toe}} := (p_{\mathrm{x}} - l_{\mathrm{f}}\cos(\phi), p_{\mathrm{y}} - l_{\mathrm{f}}\sin(\phi))^T, \quad (4)$$

$$\implies A_{\mathrm{toe}} = \begin{pmatrix} 1 & 0 & l_{\mathrm{f}}\sin(\phi) & 0 & 0 \\ 0 & 1 & -l_{\mathrm{f}}\cos(\phi) & 0 & 0 \end{pmatrix}.$$

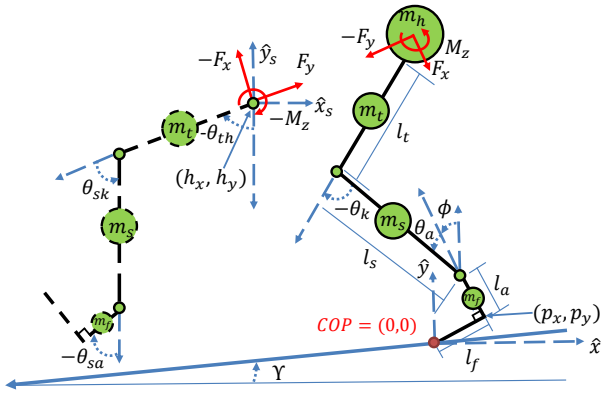

Fig. 1. Kinematic model of the biped, where the stance leg is shown in solid black and the swing leg in dashed black. For the simulation study, we assume the biped is walking on a slope with angle γ.

B. Swing Leg Dynamics

We choose the hip as a floating base for the swing leg's kinematic chain in Fig. 1. The full configuration of this leg is given as $q_{\mathrm{sw}} = (h_{\mathrm{x}}, h_{\mathrm{y}}, \theta_{\mathrm{th}}, \theta_{\mathrm{sk}}, \theta_{\mathrm{sa}})^T$, where h_{x} and h_{y} are the positions of the hip, θ_{th} is the absolute angle defined between the vertical axis and the swing thigh, and θ_{sk} and θ_{sa} are the angles of the swing knee and ankle, respectively. By deriving the equations of motion, we obtain

$$M_{\mathrm{sw}}(q_{\mathrm{sw}})\ddot{q}_{\mathrm{sw}} + C_{\mathrm{sw}}(q_{\mathrm{sw}}, \dot{q}_{\mathrm{sw}})\dot{q}_{\mathrm{sw}} + N_{\mathrm{sw}}(q_{\mathrm{sw}}) = B_{\mathrm{sw}}u_{\mathrm{sw}} + B_{\mathrm{h}}v_{\mathrm{sw}} - J_{\mathrm{sw}}(q_{\mathrm{sw}})^T F, \quad (5)$$

where M_{sw} is the inertia/mass matrix, C_{sw} is the Coriolis/centrifugal matrix, N_{sw} is the gravitational forces vector. The matrix $B_{\mathrm{sw}} = (0_{1\times 4}, 1)^T$ maps the orthosis torque

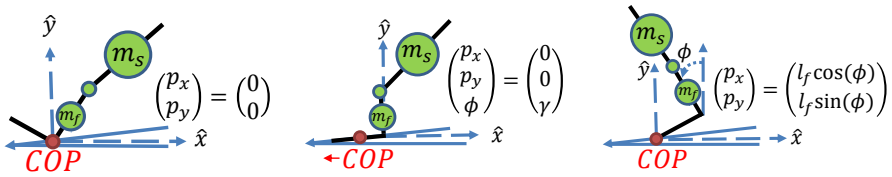

Fig. 2. Heel contact configuration (left), flat foot configuration (center), and toe contact configuration (right) during stance phase on a slope with angle γ.

u_{sw} into the system. The vector F contains the interaction forces between the swing leg and hip (including human hip torques), and $J_{\text{sw}}(q_{\text{sw}}) \in \mathbb{R}^{3\times 5}$ maps F into the dynamics. The human input vector $v_{\text{sw}} = [v_{\text{sk}}, v_{\text{sa}}]^T \in \mathbb{R}^{2\times 1}$ contains human knee and ankle torques v_{sk} and v_{sa}, respectively, which are mapped into the coordinate system through B_{h}. There are no contact constraints during swing, i.e., $A_{\text{sw}} = 0$.

III. Potential Energy Shaping Control

A. Equivalent Constrained Dynamics

In this section we will express the equations of motion as *equivalent constrained dynamics* in order to derive an underactuated control law that achieves the desired potential energy for a given contact condition [12], [13]. For the sake of generality we drop the subscripts associated with specific contact conditions. To begin we calculate the Lagrange multiplier λ based on the results in [14], [15] as

$$\begin{aligned} \lambda &= \hat{\lambda} + \tilde{\lambda}u + \bar{\lambda}F, \\ \hat{\lambda} &= W(\dot{A}\dot{q} - AM^{-1}(C\dot{q} + N - B_{\text{h}}v)), \\ \tilde{\lambda} &= WAM^{-1}B, \\ \bar{\lambda} &= WAM^{-1}J^T, \\ W &= (AM^{-1}A^T)^{-1}. \end{aligned} \tag{6}$$

Plugging in λ and A, dynamics (1) become:

$$M_\lambda \ddot{q} + C_\lambda \dot{q} + N_\lambda = B_\lambda u + B_{\text{h}\lambda} v + J_\lambda^T F, \tag{7}$$

where

$$\begin{aligned} M_\lambda &= M, \\ C_\lambda &= [I - A^T WAM^{-1}]C + A^T W\dot{A}, \\ N_\lambda &= [I - A^T WAM^{-1}]N, \\ B_\lambda &= [I - A^T WAM^{-1}]B, \\ B_{\text{h}\lambda} &= [I - A^T WAM^{-1}]B_{\text{h}}, \\ J_\lambda &= J[I - A^T WAM^{-1}]^T. \end{aligned} \tag{8}$$

We wish to use control input u to transform the open-loop dynamics (7) into closed-loop dynamics of the form

$$M_\lambda \ddot{q} + C_\lambda \dot{q} + \tilde{N}_\lambda = B_{\text{h}\lambda} v + J_\lambda^T F, \tag{9}$$

where

$$\tilde{N}_\lambda = [I - A^T WAM]^{-1}\tilde{N}, \tag{10}$$

given the desired gravitational forces vector $\tilde{N}$ that will be introduced later. Based on the results in [12] and [13], the desired dynamics (9) can be achieved in closed loop if the following *matching condition* is satisfied:

$$B_\lambda^\perp (N_\lambda - \tilde{N}_\lambda) = 0. \tag{11}$$

The underactuated potential shaping control law is then

$$u = (B_\lambda^T B_\lambda)^{-1} B_\lambda^T (N_\lambda - \tilde{N}_\lambda). \tag{12}$$

During swing we have $A_{\text{sw}} = 0$, hence (11) and (12) reduce to the classical matching condition and control law in [11].

B. Matching Conditions for Stance

We choose $\tilde{N}_{\text{st}}$ in (10) by replacing the gravitational constant in N_{st} with $\tilde{g} < g$ for BWS and $\tilde{g} > g$ for reverse BWS. Recall that the upper body segments are lumped into a single point mass at the top of the stance leg (the hip) in the stance model. Assuming the stance knee is rigid enough to provide a lever arm from the ankle to the hip, ankle torques will directly map to forces along the stance leg, which can be used to shape the weights along that leg. We approximate a rigid stance knee by setting its angle to zero, i.e., $\theta_{\text{k}} = 0$, in the potential energy before deriving the gravitational forces vector N_{st} that is used to evaluate the matching condition (11) and calculate the control law (12). As a consequence, the fifth row in N_{st}, corresponding to the knee DOF, vanishes.

We now prove for each contact condition that the weights of the stance shank, thigh, and hip can be shaped by the orthosis ankle actuator with control law (12). This control law will be identical between stance contact conditions [13], so the experimental implementation in Section IV will not need to detect specific phases of stance.

1) Heel Contact: We will simplify the multiplication between A_{heel} and M_{st}^{-1} with blockwise inversion as in [12]. Define the top-left, top-right, and bottom-right submatrices of M_{st} as $M_1 \in \mathbb{R}^{2\times 2}$, $M_2 \in \mathbb{R}^{2\times 3}$, and $M_4 \in \mathbb{R}^{3\times 3}$, respectively. Following the derivation in [12], [13]:

$$B_{\lambda 1} = \begin{bmatrix} V_1 B_{\text{st}(3,5)} \\ B_{\text{st}(3,5)} \end{bmatrix} = \begin{bmatrix} V_{12} P \\ 0 \\ P \end{bmatrix}, \tag{13}$$

$$N_{\lambda 1} = \begin{bmatrix} V_1 N_{\text{st}(3,5)} \\ N_{\text{st}(3,5)} \end{bmatrix} = \begin{bmatrix} V_{11} N_{\text{st}(3,3)} + V_{12} N_{\text{st}(4,5)} \\ N_{\text{st}(3,3)} \\ N_{\text{st}(4,5)} \end{bmatrix},$$

where $V_1 = [V_{11},\ V_{12}] = M_2 M_4^{-1}$, $V_{11} \in \mathbb{R}^{2\times 1}$, $V_{12} \in \mathbb{R}^{2\times 2}$, and $P = [1, 0]^T$. The subscript (k, z) indicates rows k through z of a matrix.

Let $\tilde{N}_{\lambda 1}$ be the desired (constrained) gravitational forces vector defined by (10). We choose the annihilator of $B_{\lambda 1}$ as

$$B_{\lambda 1}^\perp = \begin{bmatrix} I_{2\times 2} & 0_{2\times 1} & -V_{12} \\ 0_{1\times 2} & 1 & 0_{1\times 2} \\ 0_{1\times 2} & 0 & P^\perp \end{bmatrix}, \tag{14}$$

where $P^\perp = [0, 1]$ is used as an annihilator for P. Plugging terms into (11), the matching condition holds if $\tilde{N}_{\text{st}(3,3)} =$

$N_{\mathrm{st}(3,3)}$, i.e., not shaping the heel orientation DOF. Therefore the control law is defined by (12) after satisfying the matching condition with this assumption.

2) Flat Foot: At this configuration let $M_1 \in \mathbb{R}^{3\times3}$, $M_2 \in \mathbb{R}^{3\times2}$, and $M_4 \in \mathbb{R}^{2\times2}$. The same procedure yields

$$B_{\lambda 2} = \begin{bmatrix} V_2 P \\ P \end{bmatrix},\ N_{\lambda 2} = \begin{bmatrix} V_2 N_{\mathrm{st}(4,5)} \\ N_{\mathrm{st}(4,5)} \end{bmatrix}, \tag{15}$$

where $V_2 = M_2 M_4^{-1} \in \mathbb{R}^{3\times2}$. The control law is given by (12) after satisfying (11) with the annihilator

$$B_{\lambda 2}^{\perp} = \begin{bmatrix} I_{3\times3} & -V_2 \\ 0_{1\times3} & P^{\perp} \end{bmatrix}. \tag{16}$$

3) Toe Contact: At the toe contact configuration we decompose M_{st} as in the *Flat Foot* case to simplify the derivation. With the same procedure we obtain

$$B_{\lambda 3} = \begin{bmatrix} V_4 P \\ P \end{bmatrix},\ N_{\lambda 3} = \begin{bmatrix} V_3 N_{\mathrm{st}(1,3)} + V_4 N_{\mathrm{st}(4,5)} \\ N_{\mathrm{st}(4,5)} \end{bmatrix}, \tag{17}$$

where V_3 and V_4 are defined as

$$\begin{aligned} &V_3 = I_{3\times3} - K, \quad V_4 = K M_2 M_4^{-1}, \\ &K = r^T (r\Delta^{-1} r^T)^{-1} r \Delta^{-1}, \\ &r = \begin{pmatrix} 1 & 0 & l_f \sin(\phi) \\ 0 & 1 & -l_f \cos(\phi) \end{pmatrix}. \end{aligned}$$

We choose the annihilator of $B_{\lambda 3}$ as

$$B_{\lambda 3}^{\perp} = \begin{bmatrix} I_{3\times3} & -V_4 \\ 0_{1\times3} & P^{\perp} \end{bmatrix}. \tag{18}$$

Plugging in (17) and (18), the left-hand side of (11) is

$$B_{\lambda 3}^{\perp}(N_{\lambda 3} - \tilde{N}_{\lambda 3}) = V_3 (N_{\mathrm{st}(1,3)} - \tilde{N}_{\mathrm{st}(1,3)}). \tag{19}$$

The matching condition is not satisfied unless we assume $\tilde{N}_{\mathrm{st}(1,3)} = N_{\mathrm{st}(1,3)}$, i.e., not shaping the unactuated DOF ϕ (recall that p_{x} and p_{y} are constrained). The same terms can be shaped across all stance contact conditions, which can be achieved by a single control law (12) during the stance period. This control law does not depend on joint velocities or inertia matrix terms after simplification [13]. These properties will be beneficial for experimental implementation.

C. Matching Condition for Swing

For the swing leg, there are no contact constraints defined in the dynamics so the matching condition simplifies. We replace g with $\tilde{g}$ in N_{sw} to define the desired gravitational forces vector $\tilde{N}_{\mathrm{sw}}$. Letting $B_{sw}^{\perp} = [I_{4\times4}, 0_{4\times1}]$, we have $B_{\mathrm{sw}}^{\perp} B_{\mathrm{sw}} = 0$ and $\mathrm{rank}(B_{\mathrm{sw}}^{\perp}) = 4$. The left-hand side of the matching condition (11) with $A_{\mathrm{sw}} = 0$ is

$$B_{\mathrm{sw}}^{\perp}(N_{\mathrm{sw}} - \tilde{N}_{\mathrm{sw}}) = (N_{\mathrm{sw}(1,4)} - \tilde{N}_{\mathrm{sw}(1,4)}).$$

The matching condition can be satisfied if the first four rows of N_{sw}, which correspond to unactuated DOFs, are unshaped: $\tilde{N}_{\mathrm{sw}(1,4)} = N_{\mathrm{sw}(1,4)}$. Only links distal to the swing actuator can be shaped, i.e., the foot mass. This could assist individuals with weakened dorsiflexors (i.e., drop foot). Given $A_{\mathrm{sw}} = 0$, the swing controller reduces from (12) to

$$u_{\mathrm{sw}} = (B_{\mathrm{sw}}^T B_{\mathrm{sw}})^{-1} B_{\mathrm{sw}}^T (N_{\mathrm{sw}} - \tilde{N}_{\mathrm{sw}}), \tag{20}$$

where $\tilde{N}_{\mathrm{sw}} = [N_{\mathrm{sw}(1,4)}^T, \tilde{N}_{\mathrm{sw}(5)}^T]^T$.

D. Passive Walking Model

In order to understand the torques required for the potential energy shaping strategy, we will simulate it on human-like biped model, i.e, combining the stance and swing legs together in Fig. 1. The full biped model's configuration space is given as $q_{\mathrm{e}} = (q_{\mathrm{st}}^T, \theta_{\mathrm{h}}, \theta_{\mathrm{sk}}, \theta_{\mathrm{sa}})^T$, where the hip angle θ_{h} is defined between the stance and swing thighs. For simplicity we assume symmetry in the full biped, i.e., identical orthoses on both human legs [14]. We adopt the same impedance control paradigm used in [12] and [13] for the human inputs to generate a human-like walking gait, on which we test the orthosis controller. The total input torque vector for the full biped model, including orthotic and human inputs, is

$$\begin{aligned} &\tau = (B_{\mathrm{st}}^T, 0_{1\times3})^T u_{\mathrm{st}} + (0_{1\times3}, B_{\mathrm{sw}}^T)^T u_{\mathrm{sw}} + v, \\ &v = [0_{1\times3}, v_{\mathrm{a}}, v_{\mathrm{k}}, v_{\mathrm{h}}, v_{\mathrm{sk}}, v_{\mathrm{sa}}]^T \in \mathbb{R}^{8\times1}, \end{aligned} \tag{21}$$

where u_{st} is the stance controller given by (12), and v is the vector of human inputs including the hip input v_{h}. The human torque for a single joint in v is given by

$$v_j = -K_{\mathrm{p}j}(\theta_j - \theta_j^{\mathrm{eq}}) - K_{\mathrm{d}j}\dot{\theta}_j, \tag{22}$$

where $K_{\mathrm{p}j}$, $K_{\mathrm{d}j}$, θ_j^{eq} respectively correspond to the stiffness, viscosity, and equilibrium angle of joint $j \in \{\mathrm{a}, \mathrm{k}, \mathrm{h}, \mathrm{sk}, \mathrm{sa}\}$.

Biped locomotion is modeled as a hybrid dynamical system which includes continuous and discrete dynamics. Impacts happen when the swing heel contacts the ground and when contact constraints change between the heel contact and flat foot configurations. Note that no impact occurs when switching between the flat foot and toe contact configurations, but the location of the IRF does change from heel to toe. Based on [16], the hybrid dynamics and impact maps during one step are computed in the following sequence:

1. $M_{\mathrm{e}}\ddot{q}_{\mathrm{e}} + Q_{\mathrm{e}} + A_{\mathrm{e_{heel}}}^T \lambda_{\mathrm{e}} = \tau$ if $a_{\mathrm{e_{flat}}} \neq 0$,
2. $\dot{q}_{\mathrm{e}}^+ = (I - X(A_{\mathrm{e_{flat}}} X)^{-1} A_{\mathrm{e_{flat}}})\dot{q}_{\mathrm{e}}^-$ if $a_{\mathrm{e_{flat}}} = 0$,
3. $M_{\mathrm{e}}\ddot{q}_{\mathrm{e}} + Q_{\mathrm{e}} + A_{\mathrm{e_{flat}}}^T \lambda_{\mathrm{e}} = \tau$ if $|c_{\mathrm{p}}(q, \dot{q})| < l_{\mathrm{f}}$,
4. $\dot{q}_{\mathrm{e}}^+ = \dot{q}_{\mathrm{e}}^-, (q_{\mathrm{e}}(1)^+, q_{\mathrm{e}}(2)^+)^T = \mathcal{G}$ if $|c_{\mathrm{p}}(q, \dot{q})| = l_{\mathrm{f}}$,
5. $M_{\mathrm{e}}\ddot{q}_{\mathrm{e}} + Q_{\mathrm{e}} + A_{\mathrm{e_{toe}}}^T \lambda_{\mathrm{e}} = \tau$ if $h(q_{\mathrm{e}}) \neq 0$,
6. $(q_{\mathrm{e}}^+, \dot{q}_{\mathrm{e}}^+) = \Theta(q_{\mathrm{e}}^-, \dot{q}_{\mathrm{e}}^-)$ if $h(q_{\mathrm{e}}) = 0$,

where the subscript e indicates the dynamics of the full biped model, $X = M_{\mathrm{e}}^{-1} A_{\mathrm{e_{flat}}}^T$, and $\mathcal{G} = (l_{\mathrm{f}} \cos(\gamma), l_{\mathrm{f}} \sin(\gamma))^T$ models the change in IRF. The vector $c_{\mathrm{p}}(q, \dot{q})$ is the COP defined with respect to the heel IRF calculated using the conservation law of momentum. The vector Q_{e} groups the Coriolis/centrifugal terms and gravitational forces for brevity. We denote the ground clearance and ground strike impact map of the swing heel as $h(q_{\mathrm{e}})$ and Θ, respectively, based on [17]. The aforementioned sequence of continuous and discrete dynamics repeats after a complete step, i.e., phase 6 switches back to phase 1 for the next step.

E. Simulation Results

We chose average values from adult males [18] for the model parameters as in [12], [13] with trunk masses grouped at the hip. Following the same procedure presented in [12],

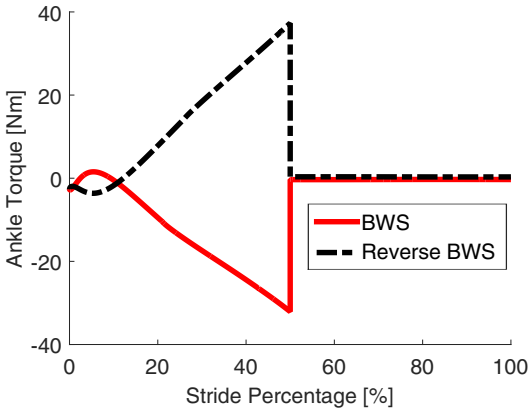

Fig. 3. Simulated ankle torque profiles for 35% BWS and reverse BWS.

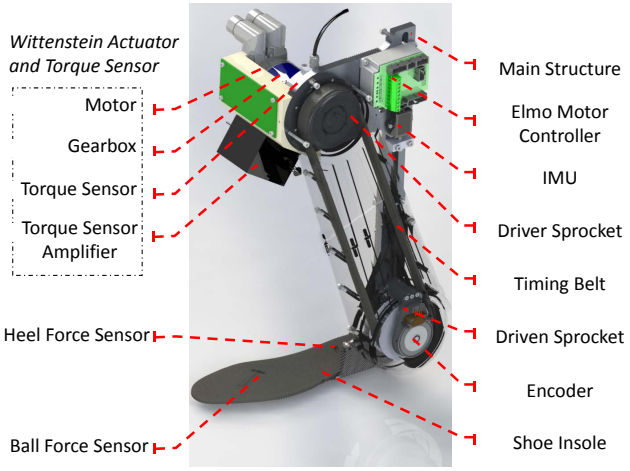

Fig. 4. Design of torque-controlled powered ankle-foot orthosis.

we first tuned the human impedance controller's gains to find a stable gait. We then implemented the energy shaping control laws for stance (Section III-B) and for swing (Section III-C). For notational purposes, 35% BWS corresponds to $\tilde{g} = 0.65g$, whereas 35% reverse BWS corresponds to $\tilde{g} = 1.35g$. The torque profiles for these conditions are shown in Fig. 3. We adopt the peak torque of about 40 Nm as a design reference for the PAFO in Section IV, though smaller BWS percentages would require smaller torques. The simulations also show that the BWS condition performs negative work on the biped (by removing potential energy), whereas the opposite holds for reverse BWS. We will similarly evaluate this effect on the human subject in Section V.

IV. Hardware Design of PAFO

We now present the design of a PAFO for testing our torque-based kinetic control strategy. Unlike kinematic control methods, kinetic control requires low backdrive torque and accurate torque tracking. The PAFO must also achieve the high torque output predicted by the simulations. These objectives were prioritized over weight and energy consumption for this control prototyping design.

A. Actuator Design

To obtain a sufficient torque output, a high torque actuator was built with a permanent magnetic synchronous motor (PMSM) and an attached two stage planetary gear transmission (TPM 004X-031x-1x01-053B-W1-999, Wittenstein, Inc.). A poly chain GT Carbon timing belt (8MGT 720, Gates Industry, Inc.) was also used to further increase the actuator output torque and to move the actuator's weight closer to the user's center of mass (which is known to minimize the metabolic burden of the added weight [19]). With an overall transmission ratio of 43.71:1, an efficiency of 0.9 and a motor peak torque of 1.29 Nm, the maximum output torque that the actuator can achieve is 50 Nm. At the same time, the actuator can provide 288 W peak power, which is sufficient for normal human walking speed under the proposed control algorithm. The combination of a high torque PMSM with a low ratio transmission was chosen to minimize backdrive torque and to provide comfort to the user. The CAD model of the powered orthosis is shown in Fig. 4.

To achieve accurate torque control performance, a PMSM with distributed winding, which has sinusoidal back-EMF [20], was selected to reduce the torque ripple and to produce smoother torque output. A field oriented motor controller (G-Sol-Gut-35/100, Elmo Motion Control, Inc.), which has less response time and torque ripple compared to trapezoidal motor control [21], was adopted to drive the motor. Hall sensors and a resolver were attached to the motor to obtain accurate position feedback for the field oriented motor controller.

B. Feedback System Design

Given the requirements of the proposed algorithm, the user's gait phase, ankle angle, and absolute shank angle were measured by the following sensors. Two force sensors (FlexiForce A301, Tekscan, Inc.) were embedded into an insole which is placed beneath the user's foot for detecting the phase of gait, e.g., stance vs. swing. These two force sensors were placed within the normal COP trajectory to provide precise readings, where one was placed under the ball of the foot, while the other one under the heel. The insole was produced on a Connex 350 3D printer and made from a rubber-like polyjet photopolymer. An optical incremental encoder (2048 CPR, E6-2048-250-IE-S-H-D-3, US Digital, Inc.) was used to obtain the ankle angle, and an Inertial Measurement Unit (3DM-GX4-25-RS232-SK1, LORD MicroStrain, Inc.) was installed on the main structure to obtain the absolute shank angle. The system was designed with a safety button that must be held continuously by the user to power the PAFO, i.e., an enable signal. The user could release the button to disable the PAFO at any point in the experiment, e.g., if balance was lost.

A reaction torque sensor (TPM 004+, Wittenstein, Inc.) was installed between the actuator case and the main structure to measure the real torque output from the actuator. The information from this sensor was used to reduce the actuator torque error caused by the nonlinear transmission efficiency, the variable motor torque constant, and the backdrive torque. Installing the torque sensor at the end of planetary gear transmission, instead of at the end of the timing belt, avoids

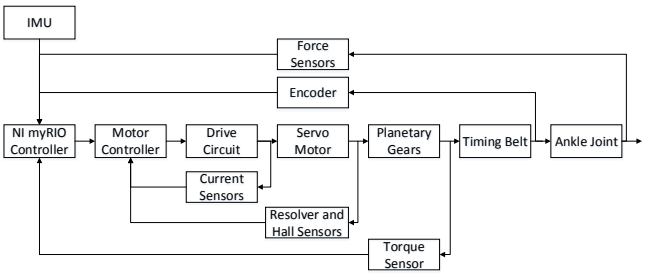

Fig. 5. Schematic of hardware system.

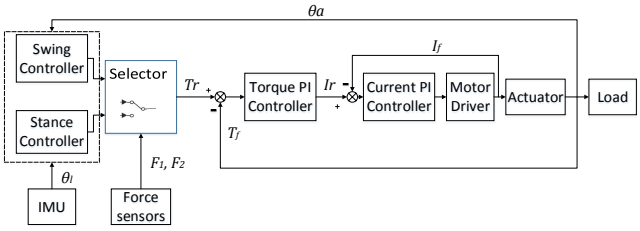

Fig. 6. Schematic of control system, where θ_a is the ankle angle, θ_l is the shank angle, F_1 and F_2 are the ground reaction forces, T_r is the torque reference, T_f is actuator torque output feedback, I_r is current reference, and I_f is motor's active current.

additional mass at the ankle joint. By measuring the torque on the actuator case, instead of the output shaft, a non-contact torque sensor can be avoided. This is beneficial since non-contact torque sensors are usually more expensive, larger in size, and heavier than the adopted reaction torque sensor. The system schematic is shown in Fig. 5.

C. Torque Control System Design

In order to provide accurate torque tracking, a torque control system was built with two closed loops (Fig. 6). The inner loop is a motor current loop that produces electromagnetic torque T_e based on the input active current as

$$T_e = (3P/2) \cdot \lambda_m \cdot i_q, \tag{23}$$

where P is the number of motor poles, λ_m is the motor flux linkage, and i_q is the active current in the d-q rotating reference frame [22].

One common methodology to realize torque control is by estimating the active current feedback, transmission ratio, and efficiency of the actuator. However, due to the nonlinear relationship between the motor winding current and the actuator output torque, an outer closed torque control loop was designed to eliminate the torque error. This torque controller tracked the reference torque commanded by the high-level control algorithm, i.e., the stance or swing controller from Section III, depending on the contact condition determined by the force sensors (Fig. 6). The closed torque control loop also compensated for the backdrive torque of the actuator, which otherwise might have a greater magnitude than the reference torque during swing and cause the user to feel resistance at the ankle. All algorithms were implemented on a real time micro-controller (myRIO-1900, National Instrument, Inc.), which has a dual-core ARM microprocessor and a Xilinx FPGA.

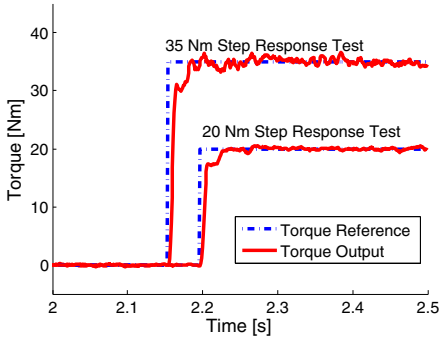

Fig. 7. Step response tracking test of the actuator control system.

D. Actuator Control System Testing

Before testing the effects of the energy shaping controller, we conducted an experiment to test the performance of torque tracking, where two reference torques, i.e., a 20 Nm step signal and a 35 Nm step signal, were given to approximate the situation when 20% or higher percentages of BWS are applied. Based on the results shown in Fig. 7, torque tracking was achieved for both experiments with steady error less than 4.5% of their torque references, respectively. This experiment validates the torque tracking loop for implementing the potential energy shaping strategy.

V. Experiments and Results

A. Experimental Setup

We experimentally tested our control algorithm on an adult male subject walking with the PAFO on a treadmill, where the experiment setup is shown in Fig. 8. For suspension the PAFO was attached to a knee brace, and the user's fit was tightened with straps. The control box worn on the subject's back contains the myRIO controller and two PCB boards for signal integration. The parameters used in the experiment are given in Table I. We estimated the mass terms of the human subject from anatomical measurements and normalized data in [23], and the mass terms of the PAFO were calculated in SolidWorks.

The human subject experiment was approved by the Institutional Review Board of UT Dallas. A safety harness was attached to the subject's torso to minimize the risk of falling. The subject was initially given time to find a natural gait with the unpowered exoskeleton on the treadmill. The subject was told not to use the handrails of the treadmill unless balance was lost. Once the subject started walking naturally with the orthosis, we started our experiments and recorded data.

We first conducted an experiment to verify the effects of backdrive torque compensation, where we let the subject wear the PAFO and walk without the energy shaping controller implemented. The experimental results are shown in Fig. 9, where the torque reference was set to zero and we switched off the torque controller after 4.6 s. The standard deviation of the backdrive torque was reduced by 58%, from 1.75 Nm to 0.75 Nm, and the mean absolute value was reduced from 1.361 Nm to 0.607 Nm. Considering the results in Fig. 7 and Fig. 9, we are unaware of any prior PAFO

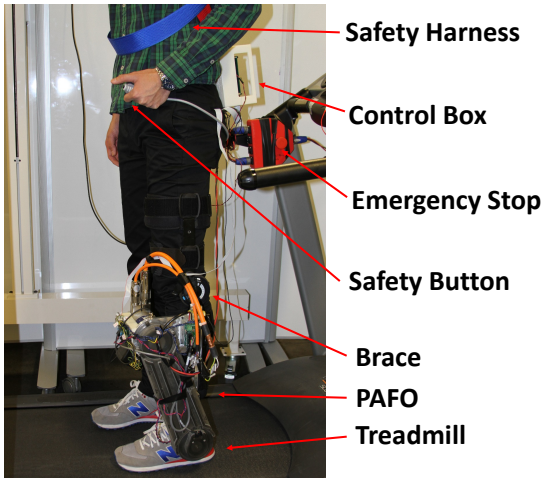

Fig. 8. Setup of the human subject experiments.

TABLE I
EXPERIMENTAL PARAMETERS

Parameter	Variable	Value
Subject Hip mass	m_{h}	42.8 [kg]
Subject Thigh mass	m_{t}	7.5 [kg]
Subject Shank mass	m_{s}	2.985 [kg]
Subject Foot mass	m_{f}	1.0875 [kg]
Subject shank length	l_{s}	0.4576 [m]
Subject thigh length	l_{t}	0.4557 [m]
Subject heel length	l_{a}	0.073 [m]
Full biped foot length	l_{f}	0.275 [m]
PAFO Shank mass	m_{so}	2.998 [kg]
PAFO Foot mass	m_{fo}	0.27 [kg]

design that can achieve such high torque and power with such low backdrive torque.

In our energy shaping experiments, we adjusted the threshold of the force sensors so that the transition between stance and swing would occur between 50% and 60% of the gait cycle. These percentages roughly correspond to the double-support period of the human gait cycle, which has a non-zero duration. However, we derived stance and swing control laws under the assumption of an instantaneous double-support period (only one foot in contact with the ground at a time). In order to ensure a smooth and safe transition between controllers, we applied a "fading process" based on the weighted sum of the stance and swing torques throughout the double support phase.

For this initial validation study we conducted two experiments with limited weight augmentation: 15% BWS and 5% reverse BWS. We stopped at 5% reverse BWS because the subject was already struggling to walk with that amount of weight addition. At the beginning of each experiment, we asked the subject to stand straight to initialize the feedback of the PAFO. Then, the subject started walking on the treadmill while holding the safety button to keep the PAFO system powered at a constant speed of 0.67 m/s. This specific walking speed was chosen based on stroke patient walking speeds, which are slower than able-bodied speeds [24]. We recorded data for 15 steps for each condition once steady

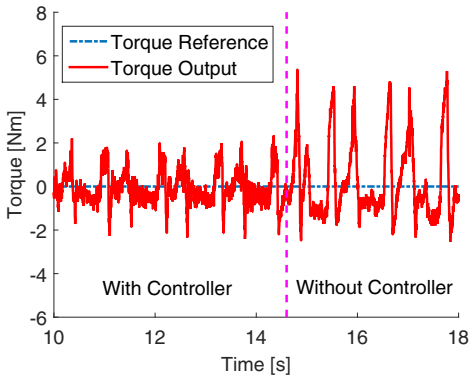

Fig. 9. Backdrive compensation during passive walking.

walking was observed. After the data was collected, the BWS condition was changed and we ran the experiment again.

B. Results and Discussion

The experimental results for 15% BWS and 5% reverse BWS are shown in Fig. 10. Each curve was calculated by taking the average of 15 steady steps, and the shaded regions represent ± 1 standard deviation about the mean. The average mechanical work done by the PAFO per stride was -8.284 J and 5.043 J for the BWS and reverse BWS conditions, respectively, confirming the removal or addition of potential energy to the human subject. A video of these experiments is available for download as supplemental multimedia.

The torque controller was able to accurately track the torque reference, where the shape of the torque profiles look similar to the simulated torque curves shown in Fig. 3. Backdrive torque was compensated by the actuator control system to minimize resistance for the subject, which can be observed in Fig. 10 during swing. Small chattering occurred during the high torques at the end of stance, which might be caused by the linear torque PI controller shown in Fig. 6. We designed the PI controller based on a linear motor model and gains of the controller were tuned to minimize torque ripple and steady state error. However, once the torque exceeded a certain threshold, the motor model became nonlinear. Hence a simple linear PI controller was not able to realize perfect tracking.

The estimated mass parameters in Table I did not need to be accurate, since the BWS percentage could be adjusted easily in the programme based on the preference of the subject. The controller did not require velocity feedback, and precise contact measurement was not needed. These experiments therefore demonstrate that the potential energy shaping control strategy can be implemented with relative ease. For both experiments, the subject was able to walk safely and comfortably with both positive and negative weight augmentation, motivating future studies with additional human subjects, including patients, to understand the effects of this weight augmentation.

VI. CONCLUSION AND FUTURE WORK

This paper presented an experimental implementation of potential energy shaping for torque control on a powered

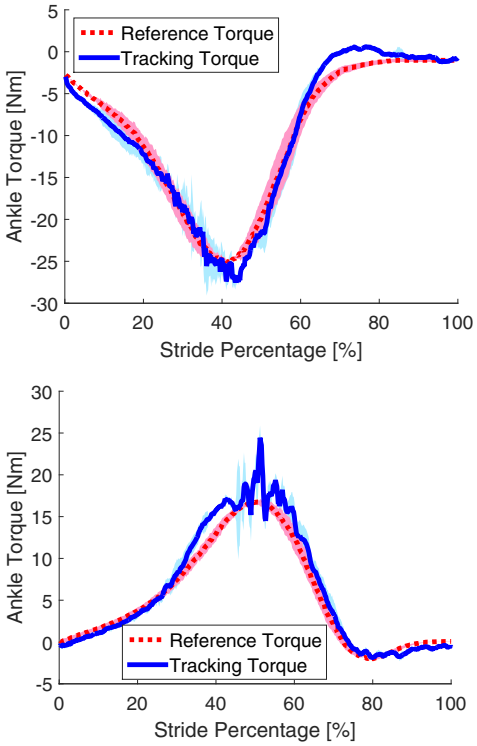

Fig. 10. Mean values (reference and tracking) and error bars (± 1 standard deviation shown in shaded regions) of the actuator torque with 15% BWS (top) and 5% reverse BWS (bottom). The blue and red error bars correspond to the tracking torque and reference torque, respectively. Part of these two shaded regions overlap.

ankle-foot orthosis. A potential energy shaping controller for the ankle actuator was derived and simulated on a biped model. Based on the simulation results, we built a highly backdrivable powered ankle-foot orthosis to implement and test this torque control strategy as a preliminary step towards a clinically relevant orthosis for stroke patients. Preliminary experiments demonstrated that the PAFO control system can track the reference torque generated by the high-level control algorithm with some tolerable tracking delay and torque ripple, which approximately matches the simulated torques.

Future work will involve multiple sets of experiments on different human subjects with different percentages of positive and negative BWS. Statistical tests can then evaluate the effects of virtual BWS on human subjects and compare these effects with the predictions of the simulations in [12], [13]. The task-invariance of the potential shaping control strategy can also be studied with experiments involving ramps and stairs. We are currently building a light-weight powered knee-and-ankle orthosis, on which we will test our control algorithms with patient subjects in the future.

Acknowledgments

The authors thank Dario Villarreal for helping us with experiments data processing.

REFERENCES

[1] T. Yan, M. Cempini, C. M. Oddo, and N. Vitiello, "Review of assistive strategies in powered lower-limb orthoses and exoskeletons," *Robotics and Autonomous Systems*, vol. 64, pp. 120–136, 2015.

[2] R. J. Farris, H. Quintero, and M. Goldfarb, "Preliminary evaluation of a powered lower limb orthosis to aid walking in paraplegic individuals," *Neural Systems and Rehabilitation Engineering, IEEE Transactions on*, vol. 19, no. 6, pp. 652–659, 2011.

[3] K. A. Strausser and H. Kazerooni, "The development and testing of a human machine interface for a mobile medical exoskeleton," in *IEEE Int. Conf. Intelligent Robots Systems*. IEEE, 2011, pp. 4911–4916.

[4] A. Duschau-Wicke, T. Brunsch, L. Lunenburger, and R. Riener, "Adaptive support for patient-cooperative gait rehabilitation with the Lokomat," in *IEEE Int. Conf. Intelligent Robots Systems*, 2008, pp. 2357–2361.

[5] D. Sanz-Merodio, M. Cestari, J. C. Arevalo, and E. Garcia, "A lower-limb exoskeleton for gait assistance in quadriplegia," in *Int. Conf. Robotics and Biomimetics*. IEEE, 2012, pp. 122–127.

[6] Y. Sankai, "Hal: Hybrid assistive limb based on cybernics," in *Robotics Research*. Springer, 2011, pp. 25–34.

[7] M. Talaty, A. Esquenazi, and J. E. Briceno, "Differentiating ability in users of the Rewalk™ powered exoskeleton: An analysis of walking kinematics," in *IEEE Int. Conf. Rehabilitation Robotics*, 2013.

[8] J. Hidler, D. Nichols, M. Pelliccio, K. Brady, D. D. Campbell, J. H. Kahn, and T. G. Hornby, "Multicenter randomized clinical trial evaluating the effectiveness of the lokomat in subacute stroke," *Neurorehabilitation and Neural Repair*, vol. 23, no. 1, pp. 5–13, 2009.

[9] M. R. Tucker, J. Olivier, A. Pagel, H. Bleuler, M. Bouri, O. Lambercy, J. d. R. Millan, R. Riener, H. Vallery, and R. Gassert, "Control strategies for active lower extremity prosthetics and orthotics: A review," *J. of Neuroengineering and Rehabilitation*, vol. 12, no. 1, p. 1, 2015.

[10] J. Ghan, R. Steger, and H. Kazerooni, "Control and system identification for the Berkeley Lower Extremity Exoskeleton (BLEEX)," *Advanced Robotics*, vol. 20, no. 9, pp. 989–1014, 2006.

[11] G. Blankenstein, R. Ortega, and A. J. Van Der Schaft, "The matching conditions of controlled lagrangians and IDA-passivity based control," *International Journal of Control*, vol. 75, no. 9, pp. 645–665, 2002.

[12] G. Lv and R. D. Gregg, "Orthotic body-weight support through underactuated potential energy shaping with contact constraints," in *Decision and Control, 2015 54th IEEE Conference on*. IEEE, 2015.

[13] ——, "Underactuated potential energy shaping with contact constraints: Application to a powered knee-ankle orthosis," *Control Systems Techonology, IEEE Transactions on*, 2015, submitted.

[14] R. D. Gregg, T. Lenzi, L. J. Hargrove, and J. W. Sensinger, "Virtual Constraint Control of a Powered Prosthetic Leg: From Simulation to Experiments with Transfemoral Amputees." *Robotics, IEEE Transactions on*, vol. 30, no. 6, pp. 1455–1471, Dec. 2014.

[15] R. M. Murray, Z. Li, S. S. Sastry, and S. S. Sastry, *A Mathematical Introduction to Robotic Manipulation*. CRC press, 1994.

[16] R. D. Gregg and J. W. Sensinger, "Biomimetic virtual constraint control of a transfemoral powered prosthetic leg," in *American Control Conference*. IEEE, 2013, pp. 5702–5708.

[17] E. R. Westervelt, J. W. Grizzle, and D. E. Koditschek, "Hybrid zero dynamics of planar biped walkers," *Automatic Control, IEEE Transactions on*, vol. 48, no. 1, pp. 42–56, 2003.

[18] P. De Leva, "Adjustments to Zatsiorsky-Seluyanov's segment inertia parameters," *J. Biomechanics*, vol. 29, no. 9, pp. 1223–1230, 1996.

[19] R. L. Waters and S. Mulroy, "The energy expenditure of normal and pathologic gait," *Gait & Posture*, vol. 9, no. 3, pp. 207–231, 1999.

[20] T. M. Jahns and W. L. Soong, "Pulsating torque minimization techniques for permanent magnet AC motor drives-a review," *Industrial Electronics, IEEE Transactions on*, vol. 43, no. 2, pp. 321–330, 1996.

[21] J. P. John, S. S. Kumar, and B. Jaya, "Space vector modulation based field oriented control scheme for brushless DC motors," in *IEEE Int. Conf. Emerging Trends Electrical Computer Tech.*, 2011, pp. 346–351.

[22] E. Oksuztepe, Z. Omac, and H. Kurum, "Sensorless vector control of pmsm with non-sinusoidal flux using observer based on fem," *Electrical Engineering*, vol. 96, no. 3, pp. 227–238, 2014.

[23] D. A. Winter, *Biomechanics and Motor Control of Human Movement*. John Wiley & Sons, 2009.

[24] P. W. Duncan, K. J. Sullivan, A. L. Behrman, S. P. Azen, S. S. Wu, S. E. Nadeau, B. H. Dobkin, D. K. Rose, J. K. Tilson, S. Cen *et al.*, "Body-weight–supported treadmill rehabilitation after stroke," *New England Journal of Medicine*, vol. 364, no. 21, pp. 2026–2036, 2011.